Numerical study of electronic impact and radiation in sonoluminescence

Ning Xu and Long Wang
Institute of Physics, Chinese Academy of Sciences, Beijing 100080, People's Republic of China

Xiwei Hu
University of Science and Technology of China, Hefei 230026, People's Republic of China

(Received 27 May 1997; revised manuscript received 7 July 1997)

A hydrodynamic simulation of pure argon single-bubble sonoluminescence including electron collisional ionization, recombination, and radiative energy loss has been performed. We find that near the moment that the bubble reaches its minimum radius the atoms inside a very thin layer around the origin of the bubble are strongly ionized, and the light emission occurs nearly simultaneously. Therefore we conclude that multiple ionization and recombination, which mainly occur in the thin layer of plasma, play a dramatically important role in the noble gas sonoluminescence. We also find that the temperature and the intensity of luminescence are not so high as those predicted by previous models, which consider only neutral gases. [S1063-651X(98)09901-2]

PACS number(s): 78.60.Mq, 44.40.+a, 47.40.−x, 34.80.Dp

A gas bubble trapped and driven by ultrasound in water generating picosecond light emission has long been known as sonoluminescence (SL). Single-bubble sonoluminescence (SBSL) was first observed by Gaitan and Crum in 1990 [1]. Most of the recent research paid more attention to SBSL since it is localized luminescence and much simpler to study than multibubble sonoluminescence (MBSL), which is a kind of luminescence randomly caused by a large number of bubbles. Experiments have indicated that SL is very sensitive to experimental parameters, e.g., the temperature of water and the intensity of acoustic pressure [2], and is extremely sensitive to the doping with a noble gas in a single bubble [3]. Heavy water also has a dramatic effect on the spectrum of light emitted by hydrogenic gases [4]. To construe the cause of the light emission, a lot of theoretical research has been done [5–10] and thus several theories were established. Shock-induced emission is one of the dominant explanations of SL [5–7]. In this opinion shocks are formed during the collapse of the bubble boundary, which heat the gas to a high enough temperature to ionize and induce light emission. Collision-induced emission [8] and quantum vacuum radiation [9,10] are two other theoretical explanations of SL.

Previous numerical simulations show that during the collapse of the bubble wall, high temperatures up to hundreds of eV will be obtained. Under such high temperature gases will be ionized. A region of plasma should exist near the center of the bubble. In this paper we consider the processes of electronic impact with atoms and ions in order to gain a more detailed description of the inner gas motion. Because of high temperature high levels of ionization are discussed here. In such circumstances of plasma, some kinds of radiation that have been observed in a confined plasma will probably occur. It has not been clear up to now which kind of radiation SL is. Therefore we only consider bremsstrahlung to simplify the simulation.

The problem discussed here is a pure argon gas bubble in water driven by a periodic acoustic field. The bubble is hypothetically in spherical symmetry. Therefore the motion of the bubble wall can be described by the Rayleigh-Plesset equation [11]

$$R\ddot{R}+\frac{3}{2}\dot{R}^2=\frac{1}{\rho_l}[P(R,t)-P_a(t)-P_0]+\frac{R}{\rho_l c_l}\frac{d}{dt}\times[P(R,t)-P_a(t)]-4\nu\frac{\dot{R}}{R}, \tag{1}$$

where R is the bubble radius, overdots denote differentiation with respect to time, $P(R,t)$ is the gas pressure next to the bubble wall, $P_a(t)=-P_a\sin\omega_a t$ is the acoustic pressure with a circular frequency of ω_a, P_0 is the ambient pressure, ρ_l is the density of the water, c_l is the speed of sound in water, and ν is the kinematic viscosity of the water. We have neglected the surface tension and other additional terms, e.g., mass diffusion and the compressibility of the water, which might have something important to do with SL.

The motion of the inner gases is controlled by the following gas dynamics equations in the Lagrangian formulation:

$$\frac{\partial\rho}{\partial t}+\frac{\rho^2}{\rho_0\xi^2}\frac{\partial}{\partial\xi}(r^2v)=0, \tag{2}$$

$$\rho_0\frac{\partial v}{\partial t}+\frac{r^2}{\xi^2}\frac{\partial P}{\partial\xi}=0, \tag{3}$$

$$\frac{\partial e}{\partial t}+P\frac{\partial(1/\rho)}{\partial t}=-U_r, \tag{4}$$

where ρ is the gas density, ρ_0 is the initial equilibrium gas density, r is the distance from the origin of the bubble, v is the gas velocity, P is the gas pressure, and e is the internal energy per unit mass. The Lagrangian coordinate ξ is defined as

$$\xi^3=3\int_0^r\frac{\rho}{\rho_0}r^2dr. \tag{5}$$

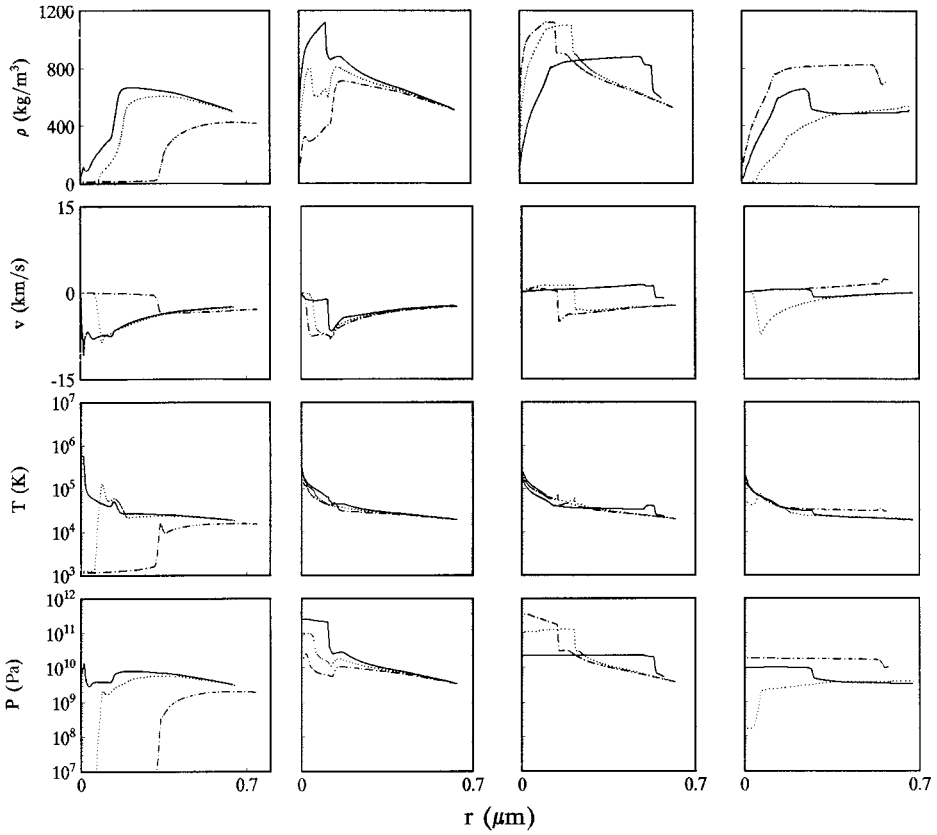

FIG. 1. The temporal evolution of density, velocity, temperature, and pressure in the pure argon gas bubble near the moment that the bubble reaches its minimum radius. The duration is 0.2907 ns, which contains twelve curves representing twelve instants. The twelve instants in turn are $t_1=22.428\,8937\ \mu$s, $t_2=t_1+0.0338$ ns, $t_3=t_1+0.0383$ ns, $t_4=t_1+0.0401$ ns, $t_5=t_1+0.0429$ ns, $t_6=t_1+0.0458$ ns, $t_7=t_1+0.0471$ ns, $t_8=t_1+0.0500$ ns, $t_9=t_1+0.0754$ ns, $t_{10}=t_1+0.0825$ ns, $t_{11}=t_1+0.2489$ ns, and $t_{12}=t_1+0.2907$ ns. The three curves in each column obey a time order of dashed line, dotted line, and solid line. The left column is with earlier instant than the right one.

The additional term U_r on the right side of Eq. (4) is the energy loss due to radiation. In order to supply $P(R,t)$ to close Eq. (1), we adopt the gas state equation, which is written as

$$P=\frac{nkT}{1-b\rho}, \tag{6}$$

$$e=\frac{3}{2}\frac{nkT}{\rho}+\frac{k}{\rho}\sum_{i=1}^{L}\sum_{j=i}^{j\leqslant L}(n_jT_i), \quad L\leqslant 18, \tag{7}$$

where $n=n_e+\Sigma_{j=0}^{L}n_j$ is the total number density of all kinds of particles, n_e is the electron number density, n_j is the number density of atoms $(j=0)$ or ions with charge of j, L is the upper critic level of the ionization that we consider in simulation, T is the gas temperature, T_i is the ionization potential of a particle with charge of $(i-1)$, k is the Boltzmann constant, and b is the van der Waals excluded volume, which avoid the gases being infinitely compressed. The two terms on the right side of Eq. (7) represent the energy of particles and the energy required for ionization. The gas density ρ and n_e, n_j are related by

$$\rho=m_en_e+\sum_{j=0}^{L}(m_jn_j), \tag{8}$$

where m_e is the mass of an electron, and m_j is the mass of an atom $(j=0)$ or an ion with a charge of j. Each kind of particle obeys

$$\frac{\partial n_j}{\partial t}+\frac{\rho n_j}{\rho_0\xi^2}\frac{\partial}{\partial\xi}(r^2v)=\dot{n}_j \quad (j=e,0,1,\ldots,L), \tag{9}$$

where $\dot{n}_j$ is the net changing rate of n_j. We treat all the particles in a fluid element with the same temperature and velocity to simplify the problem. To some degree, this simplification is reasonable.

We solve the equations above numerically in two steps, dividing the bubble radius by 800 moving points. The last point coincides with the bubble wall. The points are selected according to the Lagrangian coordinate, which makes the mass of gases between the center of the bubble and each point be fixed. The time revolutions for computation are changeable, which are determined by the conditions of the inner gas motion. In step 1, during the growth and initial collapse of the bubble wall, we use the Saha equation to obtain the number density of ions and electrons, and the time revolutions are relatively large, since no sharp changes emerge in the bubble. Step 2 starts when n_e/n_0 reaches a certain small number, which is chosen artificially. The purpose is to obtain nonzero electron density to pursue our calculation. Here we determine it to be 10^{-6}. We change the time revolutions to 10^{-3} ps and less according to the violent

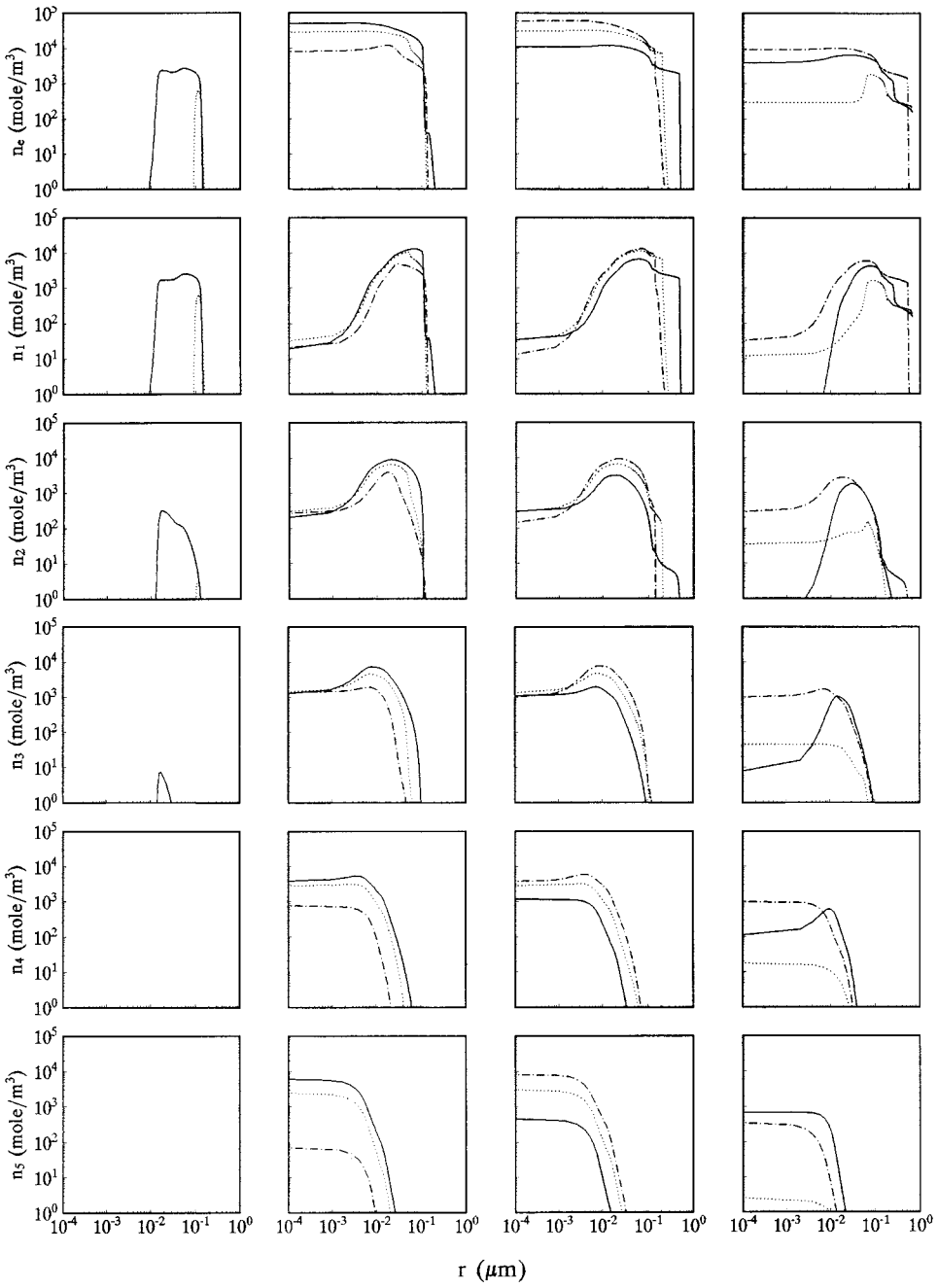

FIG. 2. The time evolution of number density of electrons and all kinds of ions that we discuss. The duration is the same as what is shown in Fig. 1. The curves also have the same time order as in Fig. 1.

motion of the gases. In this step we consider the processes of electron collisional ionization, radiative recombination, and three-body recombination. Bremsstrahlung is the only radiative energy loss that we consider. Under such condition, $\dot{n}_j$ is given by

$$\dot{n}_j = n_{j-1} n_e \alpha^{\text{ion}}_{j-1\to j} - n_j n_e \alpha^{\text{ion}}_{j\to j+1} + n_{j+1} n_e (\alpha^{\text{rrec}}_{j+1\to j} + \alpha^{\text{trec}}_{j+1\to j}) - n_j n_e (\alpha^{\text{rrec}}_{j\to j-1} + \alpha^{\text{trec}}_{j\to j-1}) \quad (j=0,1,\ldots,L), \tag{10}$$

where $\alpha^{\text{ion}}_{j\to j+1}$, $\alpha^{\text{rrec}}_{j\to j-1}$, and $\alpha^{\text{trec}}_{j\to j-1}$ represent the rates of ionization, radiative recombination, and three-body recombination of particles with charge of j. When $j=0$, the first and the fourth terms on the right side of Eq. (10) will disappear. The second and the third terms of Eq. (10) will similarly vanish for $j=L$. $\dot{n}_e$ can be obtained by the hypothesis of quasineutrality.

We assume the particles to be in Maxwellian distribution. The following are theoretical expressions of the rates we used in the simulation.

The rate of collisional ionization [12] is

$$\alpha^{\text{ion}}_{j\to j+1} = 1.86\times 10^{-7} T^{1/2} \exp(-\chi_j)[1-\exp(-\chi_j)] \times \left(\frac{I_H}{I_j}\right)^2 \Gamma \ \ [\text{cm}^3\,\text{s}^{-1}], \tag{11}$$

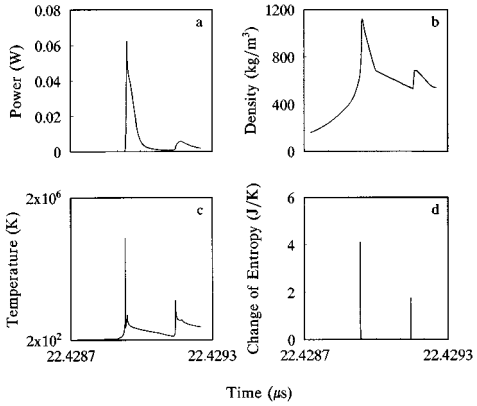

FIG. 3. The radiative power, maximum density, maximum temperature, and the change of entropy during the time interval between 22.4287 and 22.4293 μs.

where I_H and I_j are the ionization potentials (in keV) of hydrogen and an ion with charge of j or an atom ($j=0$), $\chi_j = I_j/T$, and Γ is the Gaunt factor.

The rate of radiative combination [13] is

$$\alpha^{\mathrm{rrec}}_{j\to j-1} = -1.8645\times 10^{-12}(j)^4 (M_j c^2)^{-1/2}(kT)^{-3/2} e^{1/\chi} \times E_i\left(-\frac{1}{\chi}\right) S(\chi) \ \ [\mathrm{cm^3\,s^{-1}}], \tag{12}$$

where $\chi = kT/E_{sj}$, $E_{sj} = \frac{1}{2}(j/\alpha)^2 M_j c^2$, M_j is the reduced mass of an electron and an ion with charge of j, $\alpha = 1/137.036$ is the fine-structure constant, and

$$S(x) = \begin{cases} 0.704 - 1.146 \log_{10}\chi, & \text{if } \chi \leqslant 10^{-2}, \\ 1.592 - 0.340 \log_{10}\chi + 0.113 (\log_{10})^2 \chi \\ \quad -0.031 (\log_{10})^3 \chi + 0.003 (\log_{10})^4 \chi, & \text{if } 10^{-2} \chi \leqslant 10^6, \\ 2.302 \chi^{-0.107}, & \text{if } \chi > 10^6, \end{cases} \tag{13}$$

$$E_i\left(-\frac{1}{\chi}\right) = -\ln\chi + \gamma + \sum_{n=1}^{\infty} \frac{(-1)^n}{n n! \chi^n}, \tag{14}$$

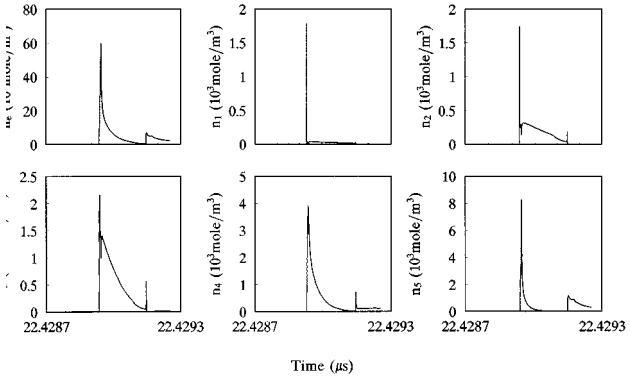

FIG. 4. The time evolution of number density of electrons and ions at the center of the bubble. The time interval is the same as what is shown in Fig. 3.

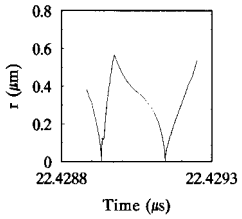

FIG. 5. The shock propagation inside the pure argon gas bubble for the case with 1.425 atm acoustic pressure.

where γ is Euler's constant.

The rate of three-body recombination [12] is

$$\alpha^{\mathrm{trec}}_{j\to j-1} = \frac{5.25\times 10^{-27}}{T^{3/2}} n_e \frac{g_j}{g_{j-1}} \exp(I_{j-1}/T)\, \alpha^{\mathrm{ion}}_{j-1\to j} \ \ [\mathrm{cm^3\,s^{-1}}], \tag{15}$$

where the g's are statistical weights.

The equilibrium radius of the bubble in our simulation is 4.5 μm. We consider such a case: $P_0 = 1$ atm, $P_a = 1.425$ atm, $\omega_a/2\pi = 26.5$ kHz, $b = 8.06\times 10^{-4}$ m^3 kg^{-1}, $\nu = 7\times 10^{-6}$ m^2 s^{-1}, $c_l = 1481$ ms^{-1}. The initial temperature in the bubble is 293 K and the ionization level L that we choose is five.

The radius of the bubble oscillates with the acoustic pressure periodically. Our focus is on a short time range around the moment when the radius reaches its minimum value. The minimum bubble radius is about 0.57 μm, which is obtained when $t \approx 22.428\,9730$ μs. Figure 1 shows the time evolution of the thermodynamic quantities and gas velocity in which we are interested during the time interval of 0.2907 ns beginning from $t = 22.428\,8937$ μs. For every variable we draw twelve curves corresponding to twelve instants. In this figure, each column contains three curves, standing for spatial profiles of different instants. The time order of these curves is the dashed line, dotted line, and solid line. There is also a time sequence among the four columns. We find that two shocks generate and reflect from the origin of the bubble before the minimum bubble radius. The temperature attains about 120 eV after the divergence of the first shock.

The time evolution of the number density of electrons and ions is shown in Fig. 2. The curves here in turn correspond to what are shown in Fig. 1. We can see that along with the increase of temperature, atoms are strongly ionized. After the first shock explosion, almost all the atoms are ionized. In a very thin layer around the center of the bubble, which is about 0.01 μm thick, multiple ionization is dramatic. The ions with higher charge offer the main part of the total number of electrons within such a thin layer. The inner gases are consequently in a state of plasma with extremely high density and pressure, as shown in Fig. 1. The high temperature and high density of charged particles cause bremsstrahlung. When the temperature drops, ions and electrons recombine. Accompanying with recombination, radiation will also take place to release the energy. The processes of radiation must be extraordinarily complex due to high density and pressure. Therefore only considering bremsstrahlung may not be sufficient. However, it can reflect some respects that are helpful for us to study SL.

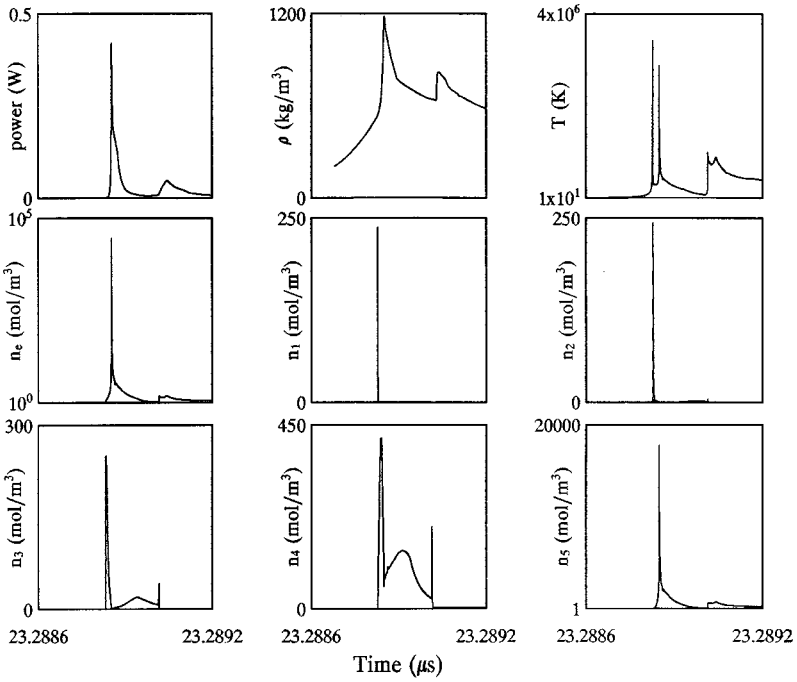

FIG. 6. The time evolution for the case that the bubble is driven by 1.5 atm acoustic pressure. The duration is about 0.6 ns starting from 23.2886 μs.

Figure 3(a) shows the evolution of radiative power caused by bremsstrahlung. The spike is about 60 mW and the duration is about 26 ps, which is obtained approximately 32 ps before the bubble reaches its minimum radius. Figures 3(b) and 3(c) present the maximum density and maximum temperature of the gases as functions of time. The density attains more than 1000 kg/m^3, which is larger than water, and the maximum temperature is about 120 eV. Figure 3(d) shows the change of entropy at the center of the bubble. A dramatic increase of entropy occurs when the gases undergo sharp changes.

Figure 4 shows the time evolution of electron and ion density at the center of the bubble. It is obvious that atoms are highly ionized during a short time interval and recombine swiftly as the temperature drops down. Figure 5 shows the shock propagation, which delineates the motion of the shock front. Referring to these two figures, we can see that at the time immediately after the shock reflection, the number of ions of Ar^{5+} is the greatest amount among all the ions that we concerned with. We have simulated other cases by changing the amplitude of the acoustic field and found that as the amplitude increases, multiple ionization plays a more and more important role in the contribution of the total electron number.

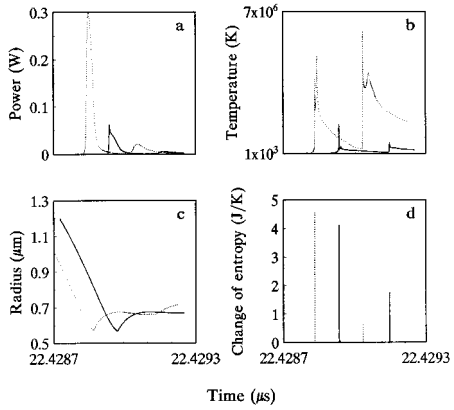

FIG. 7. The comparison of cases involving electronic impact and radiation (EIR) and involving neither (NEIR). The acoustic pressure is 1.425 atm. The dotted lines represent the NEIR model and the solid lines represent the EIR model.

The results shown in Fig. 6 are obtained by changing the acoustic pressure to 1.5 atm, which also come from the center of the bubble. In this case, nearly all the atoms are ionized to be ions of Ar^{5+} near the minimum bubble radius. Therefore ions with a charge of six or more should be included in such a simulation. The radiative power has a peak of about 0.42 W and the maximum temperature is nearly 300 eV. These values are larger than those obtained in the case discussed above. It is consistent with the parameter sensitivity to the acoustic pressure observed in experiments. Two distinct thermal spikes emerge before the maximum power output. The calculation shows that the second thermal spike appears simultaneously with the maximum density of Ar^{5+} and electrons at a time of less than one-half of a picosecond prior to the maximum light emission. This means that the ions with high charges contribute the main part of the luminescence.

During the processes of inelastic electronic impact with atoms or ions, the kinetic energy of particles has to be converted to ionization energy. The results are the increase of particle number and the drop of temperature. The involving of radiation also results in such influence. In Fig. 7 we compare the model including electronic impact and radiation (EIR) with the one not considering these two effects (NEIR). The solid lines represent the results obtained by the EIR model and the dotted lines are drawn for the NEIR model. Figure 7(c) shows the evolution of radii near the minimum

value. We can see from Fig. 7 that the instant when the bubble reaches its minimum radius delays in the EIR model and the instants that gases undergo sharp changes of different properties also lag behind those in the NEIR model. We used the Saha equation to determine the density of electrons and ions in the NEIR model in order to calculate the emitted power. Figures 7(a) and 7(b) show that the radiative power and the maximum temperature obtained by the NEIR model is much larger than those gained by the EIR model. In the NEIR model the second thermal spike shown in Fig. 7(b) is higher than the previous one, while the EIR model has the contrary conclusion. This should be attributed to the effect of involving radiative energy loss in the EIR model. Due to the generating of different kinds of ions and electrons, the second obvious change of entropy in the EIR model is larger than that in the NEIR model, which is shown in Fig. 7(d).

In this paper we have recommended a method to reveal the detailed processes of single bubble sonoluminescence theoretically. Unlike previous models, our model stresses the study of nonequilibrium. The motion of the inner gases including ionization and recombination has been delineated. Shock is still the cause of heating in our opinion. Two main shocks propagate in our work before the maximum light emission, and become remarkable as the amplitude of the acoustic field increases, which cause the appearance of two distinct thermal spikes. The inclusion of radiation and electronic impact leads to the descendence of temperature compared with the previous work, e.g., Wu and Roberts' model [5]. The results show that near the minimum bubble radius the gases undergo strong multiple ionization and sharp recombination. Moreover, as the amplitude of the acoustic field increases, the emitted power grows larger, the maximum temperature is higher, and more ions with higher charges are produced and offer the main part of the electrons. During a very short time interval, in a very thin layer around the center of the bubble, the gases are in the state of plasma with high pressure and density, which leads to the transient flash of light. The duration of the light emission accords well with experiments. The study of the action of this kind of plasma may help us discover the mystery of sonoluminescence and should attract more attention. We believe that the strong ionization and recombination of noble gases in the plasma layer should have something to do with the extreme dependence of noble gas doping in SBSL.

In further study, we plan to include more kinds of ions that might be mainly produced in the problem. We will treat the different particles with different temperature and velocity. We will consider heat conduction and other radiative processes of plasma. And we will try to find an accurate state equation of the inner gas for the extreme conditions in SL.

[1] D. F. Gaitan and L. A. Crum, J. Acoust. Soc. Am. Suppl. 1 **87**, S141(1990); D. F. Gaitan, L. A. Crum, C. C. Church and R. A. Roy J. Acoust. Soc. Am. **91**, 3116 (1992).
[2] B. P. Barber, C. C. Wu, R. Löfstedt, P. H. Roberts, and S. J. Putterman, Phys. Rev. Lett. **72**, 1380 (1994).
[3] R. Hiller, K. Weninger, S. J. Putterman, and B. P. Barber, Science **266**, 248 (1994).
[4] R. A. Hiller and S. J. Putterman, Phys. Rev. Lett. **75**, 3549 (1995).
[5] C. C. Wu and P. H. Roberts, Phys. Rev. Lett. **70**, 3424 (1993).
[6] W. C. Moss, D. B. Clarke, J. W. White, and D. A. Young, Phys. Fluids **6**, 2979 (1994).
[7] L. Kondić, J. I. Gersten, and C. Yuan, Phys. Rev. E **52**, 4976 (1995).
[8] L. Frommhold and A. A. Atchley, Phys. Rev. Lett. **73**, 2883 (1994).
[9] C. Eberlein, Phys. Rev. A **53**, 2772 (1996).
[10] C. Eberlein, Phys. Rev. Lett. **76**, 3842 (1996).
[11] A. J. Walton and G. T. Reynolds, Adv. Phys. **33**, 595 (1984).
[12] D. E. Post *et al.*, At. Data Nucl. Data Tables **20**, 398 (1977).
[13] A. Erdas and P. Quarati, Z. Phys. D **28**, 185 (1993).